

Faraday Discussions

Accepted Manuscript



This manuscript will be presented and discussed at a forthcoming Faraday Discussion meeting. All delegates can contribute to the discussion which will be included in the final volume.

Register now to attend! Full details of all upcoming meetings: <http://rsc.li/fd-upcoming-meetings>



This is an *Accepted Manuscript*, which has been through the Royal Society of Chemistry peer review process and has been accepted for publication.

Accepted Manuscripts are published online shortly after acceptance, before technical editing, formatting and proof reading. Using this free service, authors can make their results available to the community, in citable form, before we publish the edited article. We will replace this *Accepted Manuscript* with the edited and formatted *Advance Article* as soon as it is available.

You can find more information about *Accepted Manuscripts* in the [Information for Authors](#).

Please note that technical editing may introduce minor changes to the text and/or graphics, which may alter content. The journal's standard [Terms & Conditions](#) and the [Ethical guidelines](#) still apply. In no event shall the Royal Society of Chemistry be held responsible for any errors or omissions in this *Accepted Manuscript* or any consequences arising from the use of any information it contains.

Tailoring Structure Formation and Mechanical Properties of Particle Brush Solids via Homopolymer Addition

Michael Schmitt¹, Chin Ming Hui², Zachary Urbach¹, Jiajun Yan², Krzysztof Matyjaszewski^{2*}, Michael R. Bockstaller^{1*}

- 1) Department of Materials Science and Engineering, Carnegie Mellon University, 5000 Forbes Ave., Pittsburgh, PA 15213
- 2) Chemistry Department, Carnegie Mellon University, 4400 Fifth Ave., Pittsburgh, PA 15213

correspondence: bockstaller@cmu.edu; km3b@anrew.cmu.edu

Abstract

Recent progress in the area of surface-initiated controlled radical polymerization (SI-CRP) has enabled the synthesis of polymer-grafted colloids with precise control over the architecture of grafted chains. The resulting ‘particle brush materials’ are of interest both from a fundamental as well as applied perspective because structural frustrations (associated with the tethering of chains to a curved surface) imply a sensitive dependence of the interactions between brush particles on the architecture of surface-tethered chains that offers new opportunities to design hybrid materials with novel functionalities. An important prerequisite for establishing structure-property relations in particle brush materials is to understand the role of homopolymer impurities that form, for example, by thermal self-initiation. This contribution presents a detailed discussion of the role of homopolymer additives on the structure and mechanical properties of particle brush materials. The results suggest that the dissolution of homopolymer fillers follows a two-step mechanism comprised of the initial segregation of homopolymer to the interstitial regions within the array and the subsequent swelling of the particle brush (depending on the respective degree of polymerization of brush and linear chains). Addition of even small amounts of homopolymer is found to significantly increase the fracture toughness of particle brush assembly structures. The increased resistance to failure could enable the synthesis of robust colloidal crystal type materials that can be processed into complex shapes using ‘classical’ polymer forming techniques such as molding or extrusion.

Introduction

The tethering of polymeric chains to the surface of nano-sized particles or colloids has emerged as a versatile tool to modulate the interactions and assembly behavior of particulate systems but also as a means towards nanocomposite materials with novel functionalities.¹⁻⁴ Examples include the formation of particle film and colloidal crystal structures with enhanced fracture resistance or the formation of ‘one-component’ hybrid materials with enhanced electric breakdown strength or novel phonon propagation characteristics.⁵⁻⁹ A prerequisite to harness the opportunities that are afforded by polymer-tethered particulate materials is the ability to control the architecture, *i.e.* the particle radius as well as the degree of polymerization and density of grafted chains. Among the various synthetic techniques surface-initiated controlled radical polymerizations (SI-CRP) have attracted particular interest for the synthesis of polymer-tethered particle systems because of the high level of control over molecular parameters such as degree of polymerization (N) or grafting density (σ) as well as the wide range of accessible chemistries and chain constitutions.¹⁰⁻¹² Surface-initiated atom transfer radical polymerization (SI-ATRP) has attracted particular interest due to the wide range of accessible monomer compositions and functionalities, its tolerance to impurities as well as compatibility with aqueous solvent environments.¹³⁻¹⁷

However, while SI-ATRP has proven to be a versatile synthetic tool for polymer-tethered particle materials one challenge is the possibility of side reactions such as radical termination or thermal self-initiation of monomer systems. The latter process presents a particular challenge because the formation of homopolymer impurities alters the physicochemical properties of product materials and hence complicates the elucidation of

structure-property relations in polymer-tethered particle materials. To understand the conditions favoring the thermal self-initiation (TSI) of polymers during surface-initiated polymerization, our group recently evaluated the influence of reaction parameters on TSI for the particular case of poly(methyl methacrylate) (PMMA) and polystyrene (PS) tethered silica colloids.¹⁸ It was found that the influence of TSI increased with reaction temperature and decreasing catalyst reactivity. For the case of PS-tethered particle systems a fraction of up to 23% of untethered chains was observed (depending on reaction conditions). Interestingly the presence of even small amounts of homopolymer impurities was found to result in significant toughening of particle film structures. Figure 1 illustrates the general mechanism of TSI and also summarizes the toughening effect (measured in terms of the normalized mode-1 stress intensity factor) that was observed in TSI afflicted systems.

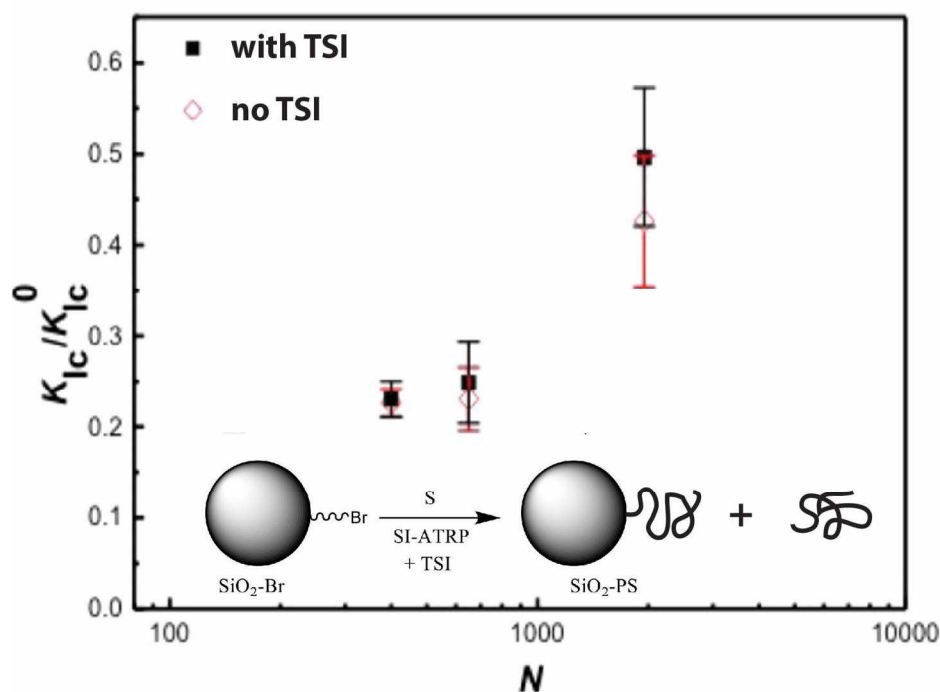


Figure 1: Dependence of the (normalized) mode-1 stress-intensity factor (fracture toughness) of $57\text{SiO}_2\text{-SN}$ thick films on the degree of polymerization of tethered chains

in the absence (red open triangles) and presence (filled black squares) of thermal self-initiation. The fracture toughness is normalized with respect to the respective value of high molecular polystyrene. The effect of thermal self-initiation (TSI) is found to increase with degree of polymerization of tethered chains. Inset illustrates mechanism of homopolymer formation by TSI. Adopted from reference 18.

The pronounced toughening in the presence of TSI that is observed in Figure 1 raises the prospect of homopolymer additives as ‘functional fillers’ to enhance the mechanical properties and processibility of polymer-tethered particle materials and thus motivates a more detailed analysis of the effect of homopolymer fillers on the structure formation and mechanical properties in polymer-tethered particle materials. The objective of the present contribution is hence to establish the effect of homopolymer addition on the order formation and micromechanical properties of polymer-tethered particle model systems as a function of both the degree of polymerization of tethered and linear chains. To limit the parameter space our focus is exclusively on densely polymer-tethered systems (that in the following will be called ‘particle brushes’). The structure of the paper is as follows: In a first part, the miscibility of homopolymer fillers within particle brush monolayers as well as its effect on the ‘degree of order’ (as determined on the basis of Voronoi tessellation analysis) will be evaluated using electron imaging. In a second part, nanoindentation will be used to assess the effect of homopolymer addition on the elastic and fracture characteristics of bulk particle brush materials.

Experimental Methods

Synthesis of Polystyrene Grafted Silica Particles Particle brush synthesis was performed using surface-initiated atom transfer radical polymerization as described

previously.^{20, 21} In a typical synthetic procedure, silica nanoparticles were modified with a tetherable initiator: 6-(triethoxysilyl)hexyl 2-bromo-2-isobutyrate for atom transfer radical polymerization (ATRP). The initiator was attached to the particle surface using NH_4OH as a catalyst in ethanol, using previously established procedures, prior to removal of excess initiator by washing with ethanol. For the polymerization, a mixture of initiator-modified silica nanoparticles ($\text{SiO}_2\text{-Br}$) and anisole was stirred in a Schlenk flask for 24 h to form a homogenous suspension. Subsequently, styrene, N,N,N',N'',N''' -pentamethyldiethylenetriamine (PMDETA) and CuBr_2 were added to the flask with a rare earth magnetic stir bar. The use of a sufficiently strong stir bar was required to prevent vitrification that can occur, especially at high monomer conversion. The solution underwent three freeze-pump-thaw cycles before being immersed in liquid nitrogen and then purged with nitrogen. Then, CuBr was added to the flask. The flask was sealed with a glass stopper and evacuated before being back-refilled with nitrogen three times. The reaction mixture was then warmed to room temperature and placed in an oil bath heated to 70°C to initiate polymerization. The final molar ratios of reaction components in a typical reaction were $[\text{Styrene}]_0:[\text{SiO}_2\text{-Br}]_0:[\text{CuBr}]_0:[\text{CuBr}_2]_0:[\text{PMDETA}]_0 = 2000:1:2.5:0.25:2.75$ with a volume fraction of non-reactive solvents of 5.4% dimethylformamide and 40% anisole in a 100 mL flask and stirred at approximately 1000 rpm. The polymerization was stopped by exposing the catalyst to oxygenated tetrahydrofuran after cooling under continuous stirring. The final product was dialyzed against tetrahydrofuran and methanol until the copper(II) catalyst was removed as evidenced by disappearance of its characteristic color.

Styrene (St, Aldrich, 99%) was purified by passing through a basic alumina column before use. Copper (I) bromide was prepared by reduction of an aqueous solution of CuBr_2 with an aqueous solution of ascorbic acid, and copper (I) chloride was prepared by reduction of CuCl_2 aqueous solution using an aqueous solution of sodium sulfite. Both copper halides were then sequentially filtered, washed with methanol, dried and stored under vacuum before use. Silica nanoparticles (SiO_2NP), 30% solution in isopropanol, effective diameter, $d_{\text{TEM}} \cong 113.2$ nm, were donated by Nissan Chemical Corporation and used as received. 5-Hexen-1-ol (98%), α -bromoisobutyryl bromide (98%), triethoxysilane (95%), ethyl 2-bromoisobutyrate (EBiB, 98%), 4,4'-dinonyl-2,2'-bipyridine (dNbpy, 99%), N,N,N',N'',N''' -pentamethyldiethylenetriamine (PMDETA, 99%), and anisole (99%) were purchased from Aldrich and used as received. All other chemicals and solvents were supplied by Aldrich and Acros Organics.

The dried product of the polymerization was redispersed in toluene, sonicated for 1 h, then stirred for 24 h before centrifugation. The centrifugation was carried out gently until the large particle brushes had sedimented at the bottom where they were collected. Removal of the free homopolymer was verified by monitoring interparticle distance via TEM.

Molecular weight and dispersity were measured by size exclusion chromatography (SEC) using a Waters 515 pump and Waters 2414 differential refractometer using PSS columns (Styrogel 10^5 , 10^3 , and 10^2 Å) in THF as an eluent (35°C , flow rate of 1 mL/min) with toluene and diphenyl ether used as internal references. A linear polystyrene (PS) standard was used for calibration. To perform SEC, chains were cleaved from particles by etching of particles in HF in a polypropylene vial

for 20 h, neutralized with ammonium hydroxide, and dried with magnesium sulfate before running SEC. Hydrofluoric acid (50 vol% HF) was purchased from Acros Organics and used as received. THF was purchased from Aldrich and used as received.

Assessment of the grafting density and inorganic content of particles were made using weight fractions measured from thermogravimetric analysis (TGA) on a Q50 TGA analyzer from TA Instruments under nitrogen up to 850°C. Grafting density was calculated by using the weight fractions measured with TGA to convert to number of polymer chains using the molar mass of polymer chains (as determined using size exclusion chromatography) and surface area (using a silica density of 2.2 g/cm³).

Transmission Electron Microscopy (TEM) Approximately monolayer films were prepared by drop casting dilute solutions (~1 mg/mL) of particle brushes and homopolymer in xylene onto poly(acrylic acid) (PAA) films. PAA was obtained as a 25 weight percent solution in water from Sigma Aldrich. The use of a low vapor pressure solvent such as xylene allowed films to better equilibrate during deposition. The films were thermally annealed at 120 °C for 24 h to fully equilibrate. The film was then placed onto a surface of water to allow the PAA substrate to dissolve. Residual particle brush films were suspended on the water surface and were lifted off onto copper grids for analysis. Particle film morphology was studied by transmission electron microscopy (TEM) with a JEOL EX2000 electron microscope operated at 200 kV. Phase and amplitude contrast mode images were taken using a Gatan Orius SC600 high-resolution camera.

Nanoindentation Elastic modulus and hardness were measured via nanoindentation. Measurements were made with an MTS Nanoindenter XP with a Berkovich tip calibrated

to a quartz standard under displacement control to no more than 10% of the nanocrystal film thickness using films (measured to be $\sim 50 \mu\text{m}$ by profilometry). Experimental data for particle brush samples were obtained from at least 20 indentations per sample, and the standard deviation of the measurements was used as experimental error. The displacement rate during the indentation of the particle brush samples was 5 nm s^{-1} to maximum load followed by constant load indentation for 10 seconds.

Atomic Force Microscopy (AFM) The residual indentations from nanoindentation were imaged using atomic force microscopy (AFM) on an NT-MDT SolverNEXT system in semi-contact mode with silicon cantilevers (300 kHz resonance frequency, 40 N m^{-1} force constant) of small tip radius ($<10 \text{ nm}$). Samples were imaged in height, phase, and deflection imaging modes in order to clearly see radial cracks at the corners of the residual indents. Cracks were most clearly observed in deflection imaging and crack lengths were measured using these images.

Results and Discussion

The systems in this study consist of low dispersity polystyrene (PS) homopolymer with degrees of polymerization, $P = 85, 442, 905$ (hereafter referred to as '10 kDa,' '50 kDa,' and '100 kDa,' respectively) as well as densely polystyrene-tethered silica particles with a particle core radius $R_0 = 56.6 \pm 6 \text{ nm}$. Homopolymers were used as purchased from Sigma-Aldrich. Silica particle brushes were synthesized using surface-initiated atom transfer radical polymerization (SI-ATRP) according to previously published protocols.¹¹

The molecular characteristics of silica brush particles were respectively: $\sigma = 0.61 \text{ nm}^{-2}$, $N = 130$, $D_M = 1.08$ (Sample ID: 57SiO₂-S130), and $\sigma = 0.49 \text{ nm}^{-2}$, $N = 130$, $D_M = 1.8$

(Sample ID: 57SiO₂-S1000) where σ is the density of surface grafted chains, N is the degree of polymerization, and D_M the molar-mass dispersity of the surface grafted chains. The grafting density of all particle brush systems in the present study was in the range $\sigma = 0.5 - 0.6 \text{ nm}^{-2}$, hence, all systems were considered to be in the dense grafting regime.

Effect of Homopolymer Addition on Structure Formation in Particle Brush Solids

To determine the solubility of homopolymer additive in particle brush solids, the morphology of thin films of particle brush/homopolymer blends was evaluated by analysis of electron micrographs of thin films of particle brush/homopolymer mixtures. This methodology was adopted due to the limitation of alternative techniques (such as small-angle X-ray scattering or cross-sectional imaging) that cannot be applied in the present case (due to the strong scattering of particle cores and interference of the large particles with the microtoming process, respectively). Substrate interactions might alter the distribution of components within the film; however, we expect the effect of such interactions to be of limited influence due to the identical chemical composition of brush and linear polymer. For each blend system, ten micrographs from different regions of the film (averaging about $500 \text{ }\mu\text{m}^2$) were evaluated to allow for representative sample analysis. Contrast gradient analysis was applied to differentiate homopolymer domains from void space that might form during film casting and hence to determine the miscibility of particle brush/homopolymer blend systems. Figure 2 depicts representative transmission electron micrographs of the structure formation in of 57SiO₂-S1000/10 kDa (panels a-d) 57SiO₂-S1000/100 kDa (panels e-h), 57SiO₂-S130/1000 kDa (i-l), respectively.

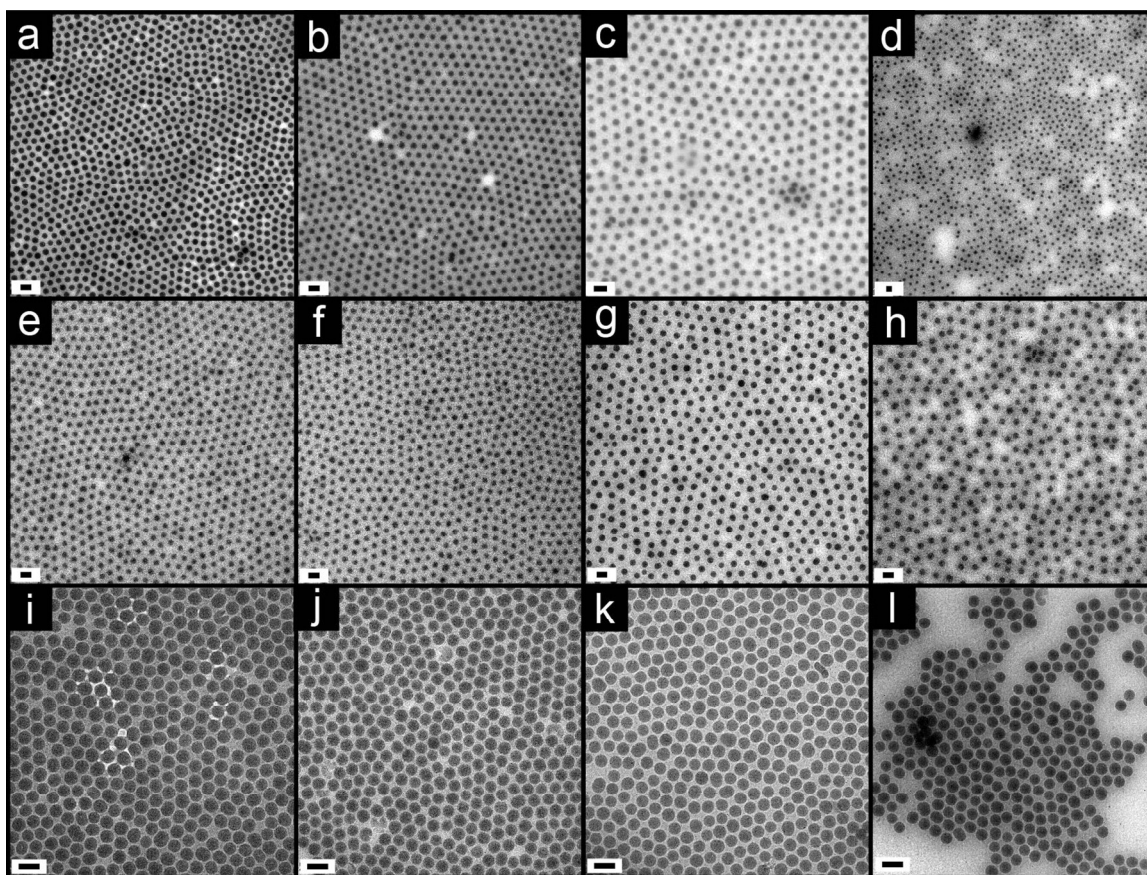


Figure 2: Representative transmission electron micrographs of 57SiO₂-S1000 blends with (a-d) 10 kDa and (e-h) 100 kDa PS and 57SiO₂-S100 blends with (i-l) 100kDa PS. Homopolymer volume fractions are (a, i) 0, (j) 0.15, (b, e, k) 0.26, (l) 0.35, (c, f) 0.41 (g) 0.51 (d, h) 0.58. For the 57SiO₂-S1000 blend systems, a significantly high solubility of homopolymer is observed as compared to 57SiO₂-S130 based systems (see text for more details). All scale bars are 250 nm.

The micrographs reveal that in the case of 57SiO₂-S1000 blend systems the particle array morphology is approximately maintained up to high concentrations of homopolymer ($\phi \sim 0.5$) while the formation of ‘patch’ structures in the case of 57SiO₂-S130/1000 kDa at low homopolymer concentration ($\phi > 0.26$) indicates a reduced solubility in this latter case. The observed trend bears analogy to prior reports on the miscibility of particle brush fillers in polymer melts that has been found to primarily depend on the ability of matrix (melt) chains to wet (interpenetrate) the brush.²¹⁻²³ Pioneering work by Leibler and

co-workers revealed the interaction between planar polymer brushes and melts is primarily dependent on three parameters: the degree of polymerization of tethered chains (N) and matrix (P) chains.²⁴⁻²⁶ Specifically, the authors determined (for the case of chemically identical brush and matrix polymers) that wetting of the brush by the matrix is subject to the condition $P < N$. Hence autophobic dewetting (and particle brush aggregation) is expected if the degree of polymerization of tethered chains is less than the matrix. More recent theoretical studies have extended the Leibler model to account for the effect of surface curvature (such as in the case of particle brushes).²⁷ Harton and Kumar found that in case of curved brushes the wetting condition follows the same general trend, however, the upper bound the degree of polymerization of matrix chains to facilitate wetting of the brush was found to increase with the curvature of the brush (*i.e.* with reduced particle size).²⁸ This latter effect was attributed to the reduced chain crowding in high curved (convex) brush systems. The role of brush and matrix degree of polymerization on the brush wetting characteristics is illustrated in Figure 3.

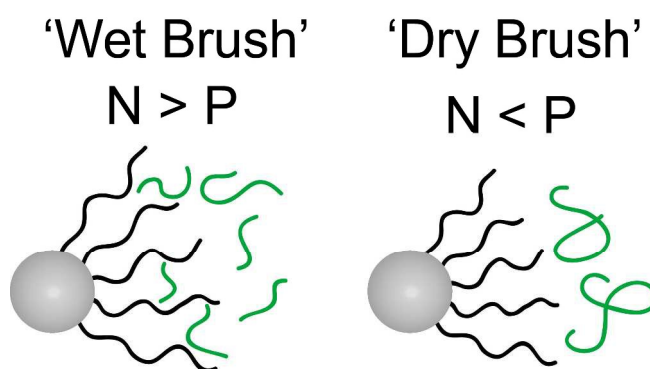


Figure 3: Wet brush behavior, where the homopolymer easily interpenetrates the graft layer, is expected when the homopolymer chain length, P , is less than the graft length, N ($P < N$). Dry brush behavior, *i.e.* the expulsion of the matrix polymer from the brush is expected when the homopolymer chain length exceeds the graft length ($P > N$).

Although the miscibility of homopolymer in particle brush films (see Fig. 2) generally follows the predicted trend for particle brush-in-polymer dispersions, it is important to note that the solubility of 100 kDa homopolymer in the 57SiO₂-S100 brush system up to concentrations of $\phi \sim 0.26$ (see Figs. 2k & 2l) is surprising since in this case $P \sim 10 \times N$ and hence strong autophobic dewetting is expected. The pronounced miscibility of high molecular homopolymer filler points to additional contributions to the free energy of mixing that are not considered in the classical brush/melt interaction model. In particular, we hypothesize that in particle brush array structures the surface energy associated with interstitial space contributes an additional driving force for mixing that is not accounted for in the classical wetting theory (since the latter has been designed to capture the wetting conditions of dilute particle brush-in polymer dispersions rather than the ‘insertion’ of polymer chains in a uniform particle brush phase). In a first approximation, the amount of void space in particle brush array structures can be estimated on the basis of a close-packed hard sphere model for which the amount of interstitial space is $\phi_{\text{void}} = 0.26$. The surface energy associated with the polymer/air interfaces across void space provides a strong energetic driving force for homopolymer filling of interstitial regions. For example, by considering the typical values for the air/PS interfacial energy ($\gamma_{\text{air-PS}} = 40 \text{ mN m}^{-1}$) it follows that the surface energy penalty per chain amounts to approximately $10^5 k_{\text{B}}T$ (assuming $N \sim 1000$ and $R_0 = 60 \text{ nm}$). In particle brush array structures the actual amount of void space will be reduced because of the stretching of tethered chains to fill the interstitial space. This latter process is energetically favored because the energy penalty associated with the reduction of chain conformational entropy during chain stretching amounts to only a small fraction of the energy gain due to the reduction of

surface energy.¹⁹ The chain stretching along the interstitial regions (that correspond to the corners of the corresponding Wigner-Seitz cell of the array) can indeed be inferred from the contrast distribution in electron micrographs or pristine particle brush arrays in Figure 2 where interstitial regions appear as ‘brighter regions’ (indicating local thinning of the film). Despite this relief of the energy associated with void spaces it can be expected that the presence of ‘interstitials’ in particle brush arrays creates ‘energy hot spots’ that will drive the segregation of homopolymer within interstitial regions (to reduce either surface energy or the stored elastic energy in the case of chain stretching). This is supported by previous reports by Ojha *et al.* who evaluated the morphology of blends of asymmetric (*i.e.* large/small) particle brush mixtures and reported small particle brushes to decorate interstitial regions.¹⁹ On the basis of the above arguments we rationalize the solubility of 100 kDa fillers within the 57SiO₂-S130 as a consequence of the initial ‘segregation’ of homopolymer within interstitial regions that is independent of brush/matrix interpenetration. Consistent with this argument we find that the solubility limit of 100 kDa PS is approximately 26 % and hence of the same order as the estimated interstitial space in the particle brush lattice.

Support for the conclusion that chain relaxation across interstitial regions drives the distribution of homopolymer in the limit of small filling fractions can be derived from the analysis of the ‘degree of order’ of particle brush array structures that is shown in Figure 4.

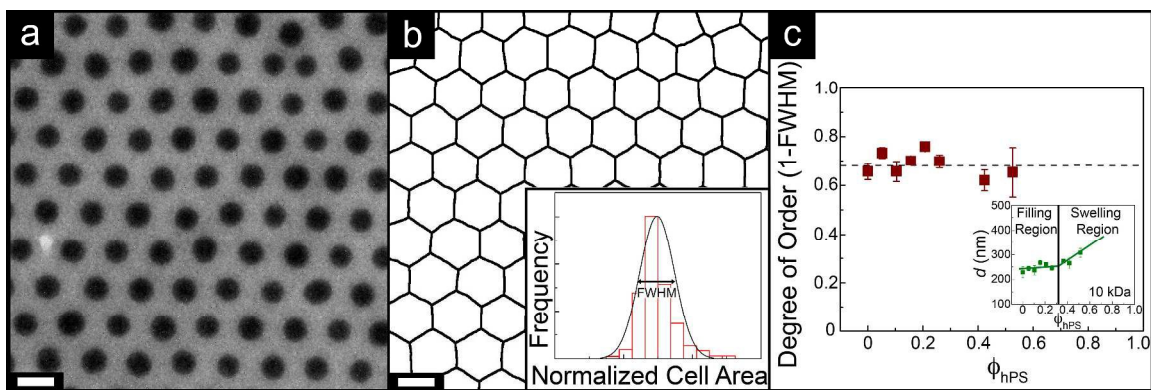


Figure 4: (a) Representative electron micrograph of the $57\text{SiO}_2\text{-S1000}$ array. (b) Corresponding Voronoi diagram used to calculate the degree of order. The degree of order is defined as 1-FWHM , where FWHM is the full-width half-maximum of a Gaussian fitted to the distribution of normalized Voronoi-cell areas calculated from the diagram (shown in inset). (c) Degrees of order for the range of soluble $57\text{SiO}_2\text{-S1000}$ and 10 kDa PS composites showing that order is retained for all homopolymer volume fractions. Inset shows that while order is maintained in all systems, interparticle distance increases faster when homopolymer volume exceeds the expected interstitial volume. Scale bars are 200 nm.

The ‘degree of order’ of particle brush monolayers (Fig. 4a) was evaluated on the basis of full-width-at-half-maximum (FWHM) of the normalized Voronoi cell area distribution (Figs. 4b and 4c) that was introduced by Choi *et al.* as a quality factor to compare order formation in brush particle systems.²⁹ Analysis of the quality factor (1-FWHM) in the case of the $57\text{SiO}_2\text{-S1000}/10$ kDa system reveals that order formation is unaffected by the presence of homopolymer filler for all experimental compositions thus confirming the solubility of the 10 kDa additive (consistent with $N \gg P$). Interestingly, the analysis of nearest neighbor surface-to-surface distance (see inset in Fig. 4c) reveals that the particle distance is approximately constant up to a threshold concentration that corresponds approximately to the estimated volume fraction of interstitial space beyond which the particle distance increases with filler concentration. This trend of particle distance is consistent with the process of homopolymer dissolution being governed by two steps: the

initial segregation of homopolymer within the interstitial regions of the array structure and the subsequent swelling of the brush (provided that $N > P$). Figure 5 illustrates the proposed two-step dissolution process.

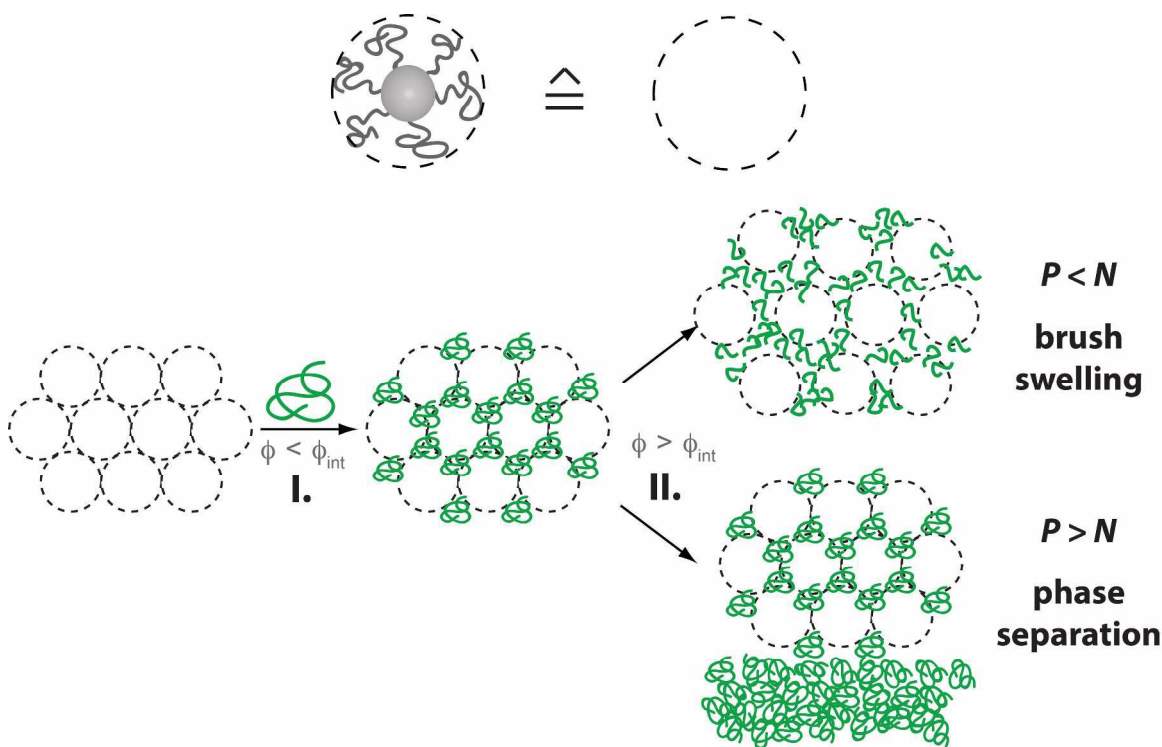


Figure 5: Illustration of the proposed two-step dissolution process of homopolymer additives in particle brush array structures. In a first step, homopolymer filler segregates to the interstitial regions of the array structure (independent of P and N). In a second step, as $\phi > \phi_{\text{int}}$ the homopolymer swells the brush (if $N > P$) or phase separates from the mixture (if $N < P$).

Mechanical Properties of Homopolymer Filled Particle Brush Solids

To evaluate the effect of homopolymer addition on the mechanical properties of particle brush solids, particle brush/polymer blends were evaluated by nanoindentation. Nanoindentation has emerged as a versatile technique to determine the micromechanical properties of materials for which macroscopic mechanical tests cannot be performed (for example because of insufficient sample amount).³⁰ Films of $\sim 50 \mu\text{m}$ thickness were

indented to a depth of 2 μm using a Berkovich indenter at a rate of 5 nm s^{-1} (rates from 1 – 25 nm s^{-1} were tested to exclude the influence of viscoelastic effects on the measurement result). Maximum displacement was limited to less than 10% of the film thickness to precluded substrate effects, for select samples the measurements were performed at varying film thicknesses to ensure consistency of results (data not shown here). Note that for the present experimental conditions, the indentation test samples a volume of about 50 μm^3 and hence the results are expected to be insensitive to microstructural defects. Figure 6 depicts typical load-displacement behaviors for a 57SiO_2 -S1000/50kDa blend system.

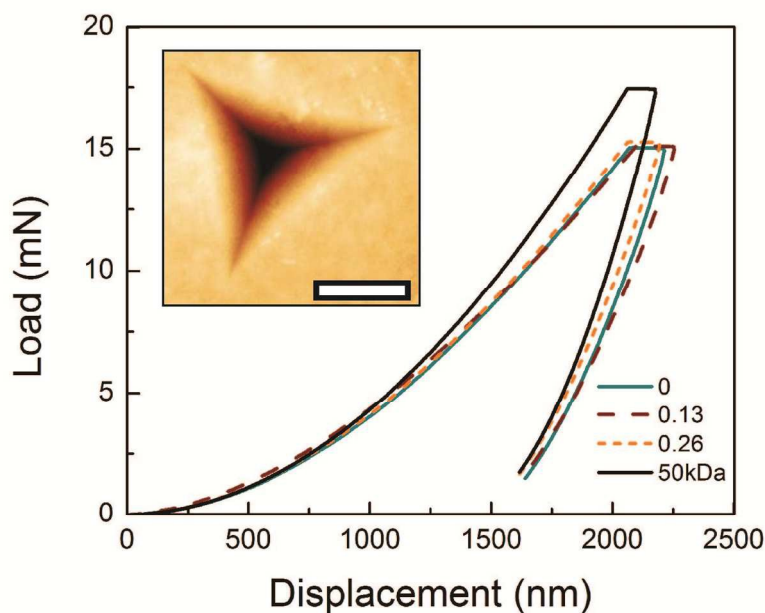


Figure 6: Characteristic load-displacement curves for the 57SiO_2 -S1000/50kDa composites with different volume fractions of homopolymer (see legend) show similar behavior to the 50kDa homopolymer filler. Inset shows a residual indent for the pristine 57SiO_2 -S1000 system revealing the absence of pile up or plastic deformation. Scale bar is 5 nm.

Because the reliable evaluation of the mechanical properties of films requires sufficient mechanical stability of films only the 57SiO₂-S1000 particle brush system was chosen for nanoindentation analysis. Furthermore, 50 kDa PS was selected as additive to facilitate both matrix/brush compatibility (*i.e.* wet brush conditions) as well as chain entanglement. From nanoindentation measurements three mechanical parameters can readily be determined under the assumption of elastic deformation behavior: the hardness H (from the maximum load level during indentation), the elastic modulus E (from the initial slope of the unloading curve) as well as the stress intensity factor for mode-1 fracture K_{Ic} (from the length of cracks that form at the indenter tip regions).^{7, 31} The latter provides a measure for the toughness of the material and hence describes the resistance of the material to fracture. Data analysis was performed on the basis of at least 20 indentations per sample to determine average values as well as experimental error. We note that the above analysis is based on the assumption of elastic deformation and hence only applicable to polymers well below the glass transition temperature. To exclude significant contributions from plastic deformation the morphology of indents was evaluated by atomic force microscopy (AFM) – the inset in Figure 6 depicts a representative micrograph of an indent. The lack of pile-up or sink-in confirms the absence of (significant) plastic deformation. To determine the stress intensity factor the length of cracks emanating from the corners of residual indentation sites were analysed using the following equation first derived by Oliver and Pharr³¹:

$$K_{Ic} = 0.0161 \left(\frac{a}{l}\right)^{\frac{1}{2}} \left(\frac{E}{H}\right)^{\frac{2}{3}} \frac{P_{\max}^{\frac{2}{3}}}{c^{\frac{3}{2}}} \quad (1)$$

Where K_{Ic} is the fracture toughness, a is the distance from the center of the residual indent to the corner, l is the length of the crack (from the indent corner to tip), c is the

total length of the crack and center-to-corner distance ($a + l$), E is the Young's modulus, H is the hardness, and P_{max} is the maximum load.³¹ The stress intensity factor was calculated based on measurements of at least 10 residual indentations. This analysis was previously used to calculate the fracture toughness of particle brushes with small particle sizes ($R_0 = 8$ nm).⁷ All error bars reported are equal to one standard deviation in the measurement value above and below the mean value.

Figure 7 depicts a summary of the mechanical properties of 57SiO₂-S1000/50kDa blend systems that were determined by indentation experiments.

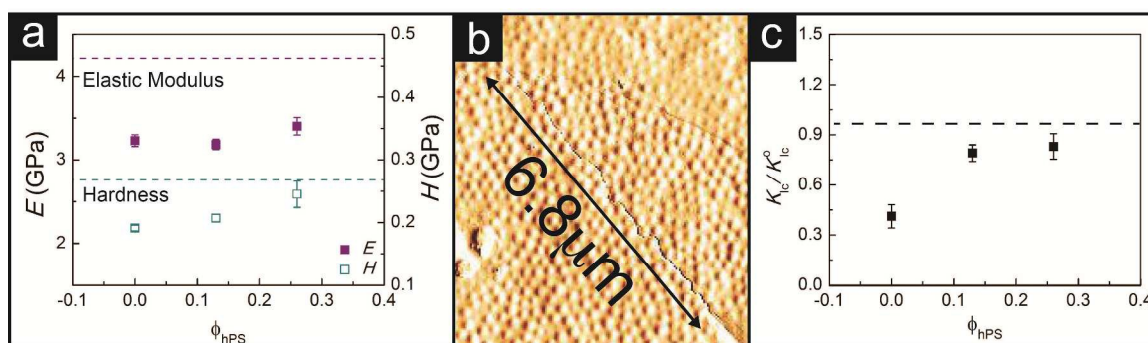


Figure 7: (a) Young's modulus and hardness of 57SiO₂-S1000 and 50kDa composites as a function of homopolymer volume fraction. Modulus and hardness show only weak dependence on the amount of added homopolymer. (b) Fracture cracks propagating from corners of the residual indent as shown for the case of 57SiO₂-S1000. Crack length is reduced upon homopolymer addition. (c) Normalized mode-1 stress intensity factor (fracture toughness, normalized with respect to the value of 100 kDa homopolymer (dashed line)) for particle brush/homopolymer blend systems. Dashed line corresponds to normalized fracture toughness of 50 kDa polystyrene.

Figure 7a reveals that Young's modulus remains approximately constant for all concentrations of added homopolymer and significantly below the respective value of the 50 kDa reference PS (black dashed line). This trend can be interpreted as a consequence of elastic deformations (i.e. Young's modulus) being evaluated in the small strain limit

where short-ranged dispersion interactions provide the major contribution to restoring force. Since dispersion interactions depend on the molecular polarizability and both the tethered and linear polymer exhibit identical chemical composition no significant change is expected in the limit of small amounts of added filler. We hypothesize that residual effects related to interstitial regions (such as void spaces) are responsible for the modulus of particle brush/homopolymer films to remain below the corresponding value of the 50 kDa homopolymer. While elastic constants show only a weak dependence on the homopolymer content, a pronounced increase of the films' fracture toughness by about 300% is observed upon addition of even small amounts of homopolymer (see Fig. 7c). Here it should be noted that fracture toughness (*i.e.* the work required to fracture a material) – in contrast to small strain elastic deformations – sensitively depends on the presence of entanglements.^{32, 33} We thus rationalize the pronounced increase of the materials fracture toughness with the increase of the materials' entanglement density as the homopolymer additive fills the interstitial regions in the array. The proposed toughening effect of 'decorated interstitial regions' is illustrated in Figure 8.

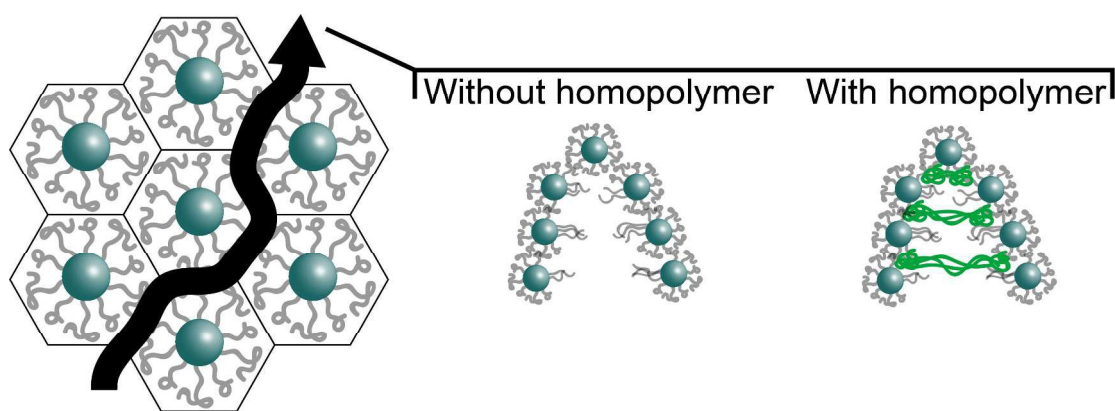


Figure 8: Illustration of the homopolymer-induced toughening effect. As a crack (shown by the thick black line) propagates through the material, the presence of entangled homopolymer in the interstitial regions introduces microscopic flow processes (*i.e.* crazing) that stabilize the crack against further propagation.

An interesting experiment to validate the above proposition would be to evaluate the effect of low molecular polymer fillers for which no entanglement formation is expected (*i.e.* in the limit of $P < N_{\text{entgl}}$). Unfortunately, despite extensive experimentation no reliable data could be obtained on these small P systems could be obtained during the course of the present study (due to the brittleness of films that rendered determination K_{1c} difficult).

Conclusions

We have analyzed the effect of homopolymer addition on the structure formation and mechanical properties of particle brush solids. In the limit of small volume fraction, homopolymer additives are soluble within the particle brush solid even for ‘dry brush’ compositions. The solubility of high molecular weight polymers that are otherwise expected to be immiscible within the brush is interpreted as a consequence of a strong driving force to fill ‘interstitial regions’ within the particle brush solid that derives from either surface energy contributions (in the case of short-chain brushes) or the recovery of relaxed chain conformations (in the case of long-chain brushes in which chain stretching prevents the formation of void space in the interstitial region). The addition of small amounts of homopolymer corresponding to only a fraction of the interstitial volume significantly raises the toughness of particle brush solids indicating chain entanglement of polymer chains that are segregated within the interstitial regions. The ability to raise the material’s fracture toughness at low concentrations of added filler (where microstructural order is unaffected by the filler addition) promises new opportunities for designing particle-brush based materials that combine the favorable ability of forming

ordered assembly structures of dense brush particles with polymer-like processability and mechanical robustness. Future work will test alternative approaches to facilitate this goal, for example, by means of bimodal particle brush systems.³⁴

Acknowledgements

M.R.B. and K.M. acknowledge financial support by the National Science Foundation (via DMR-1410845 and DMR-1501324) as well as the Department of Energy (via DE-EE0006702). M.S. gratefully acknowledges financial support from the John and Clare Bertucci Graduate Fellowship.

References

- [1] C. M. Hui, J. Pietrasik, M. Schmitt, C. Mahoney, J. Choi, M. R. Bockstaller and K. Matyjaszewski, *Chem. Mater.*, 2014, **26**, 745-762.
- [2] N. J. Fernandes, H. Koerner, E. P. Giannelis, R. A. Vaia, *MRS Comm.*, 2013, **3**, 13-29.
- [3] S. K. Kumar, N. Jouault, B. Benicewicz, T. Neely, *Macromolecules* 2013, **46**, 3199-3214.
- [4] S. L. Hilburg, A. N. Elder, H. Chung, R. L. Ferebee, M. R. Bockstaller, N. R. Washburn, *Polymer*, 2014, **55**, 995-1003.
- [5] P. Voudouris, J. Choi, N. Gomopoulos, R. Sainidou, H. Dong, K. Matyjaszewski, M. R. Bockstaller, G. Fytas, *ACS Nano* 2011, **5**, 5746-5754.
- [6] J. Choi, H. Dong, K. Matyjaszewski and M. R. Bockstaller, *J. Am. Chem. Soc.*, 2010, **132**, 12537-12539.
- [7] J. Choi, C. M. Hui, J. Pietrasik, H. Dong, K. Matyjaszewski and M. R. Bockstaller, *Soft Matter*, 2012, **8**, 4072-4080.
- [8] C. A. Grabowski, H. Koerner, S. Meth, A. Dang, C. M. Hui, K. Matyjaszewski, M. R. Bockstaller, M. F. Durstock and R. A. Vaia, *ACS Appl. Mater. Inter.*, 2014, **6**, 21500-21509.
- [9] E. Alonso-Redondo, M. Schmitt, Z. Urbach, C. M. Hui, R. Sainidou, P. Rembert, K. Matyjaszewski, M. R. Bockstaller & G. Fytas *Nat. Commun.*, 2015, **6**, 8309, 1-8.
- [10] R. Barbey, L. Lavanant, D. Paripovic, N. Schuewer, C. Sugnaux, S. Tugulu, H.-A. Klok, *Chem. Rev.*, 2009, **109**, 5437-5527.
- [11] R. Advincula, *Adv. Polym. Sci.*, 2006, **197**, 107-136.

- [12] Y. Tsujii, K. Ohno, S. Yamamoto, A. Goto, T. Fukuda, *Adv. Polym. Sci.*, 2006, **197**, 1-45.
- [13] V. Coessens, T. Pintauer, K. Matyjaszewski, *Prog. Polym. Sci.*, 2001, **26**, 337-377.
- [14] K. Matyjaszewski, *Macromolecules*, 2012, **45**, 4015-4039.
- [15] K. Matyjaszewski, N. V. Tsarevsky, *Nature Chem.*, 2009, **1**, 276-288.
- [16] K. Matyjaszewski, N. V. Tsarevsky, *J. Am. Chem. Soc.*, 2014, **136**, 6513-6533.
- [17] K. Matyjaszewski, J. Xia, *Chem. Rev.*, 2001, **101**, 2921-2990.
- [18] C. M. Hui, A. Dang, B. Chen, J. Yan, D. Konkolewicz, H. He, R. Ferebee, M. R. Bockstaller, K. Matyjaszewski, *Macromolecules*, 2014, **47**, 5501-5508.
- [19] S. Ojha, B. Beppler, H. Dong, K. Matyjaszewski, S. Garoff and M. R. Bockstaller, *Langmuir*, 2010, **26**, 13210-13215.
- [20] J.-S. Wang and K. Matyjaszewski, *J. Am. Chem. Soc.*, 1995, **117**, 5614-5615.
- [21] S. Ojha, A. Dang, C. M. Hui, C. Mahoney, K. Matyjaszewski, M. R. Bockstaller, *Langmuir*, 2013, **29**, 8989-8996.
- [22] S. K. Kumar, N. Jouault, B. Benicewicz and T. Neely, *Macromolecules*, 2013, **46**, 3199-3214.
- [23] J. F. Moll, P. Akcora, A. Rungta, S. Gong, R. H. Colby, B. C. Benicewicz, S. K. Kumar, *Macromolecules*, 2011, **44**, 7473-7477.
- [24] A. Gast, L. Leibler, *Macromolecules*, 1985, **19**, 686-691.
- [25] I. Borukhov, L. Leibler, *Macromolecules*, 2002, **35**, 5171-5182.
- [26] I. Borukhov, L. Leibler, *Phys. Rev. E*, 2000, **62**, R41-R44.
- [27] D. Meng, S. K. Kumar, J. M. D. Lane, G. S. Grest, *Soft Matter*, 2012, **8**, 5002-5010.
- [28] S. E. Harton, S. K. Kumar, *J. Polym. Sci. Pol. Phys.*, 2008, **46**, 351-358.

- [29] J. Choi, C. M. Hui, M. Schmitt, J. Pietrasik, S. Margel, K. Matyjaszewski and M. R. Bockstaller, *Langmuir*, 2013, **29**, 6452-6459.
- [30] A. C. Fischer-Cripps, *Nanoindentation 3rd ed.*, Springer, New York, 2011.
- [31] W. C. Oliver and G. M. Pharr, *J. Mater. Res.*, 2004, **19**, 3-20.
- [32] W. Graessley, *Adv. Polym. Sci.*, 1974, **16**, 1-179.
- [33] E. J. Kramer and L. L. Berger, *Adv. in Polym. Sci.*, 1990, **91/92**, 1-68.
- [34] J. Yan, T. Kristufek, M. Schmitt, Z. Wang, G. Xie, A. Dang, C. Hui, J. Pietrasik, M. Bockstaller, K. Matyjaszewski, *Macromolecules*, 2015, in press.